Published in final edited form as:

Cancer Res. 2022 August 16; 82(16): 2874–2886. doi:10.1158/0008-5472.CAN-21-4313.

PRC2 Heterogeneity Drives Tumor Growth in Medulloblastoma

Jiaqing Yi[1], **BongWoo Kim**[1], **Xuanming Shi**[1], **Xiaoming Zhan**[1], **Q. Richard Lu**[2], **Zhenyu Xuan**[3], **Jiang Wu**[1,#]

[1]Department of Physiology, University of Texas Southwestern Medical Center, Dallas, TX 75390, USA

[2]Brain Tumor Center, Cincinnati Children's Hospital Medical Center, Cincinnati, Ohio, USA.

[3]Department of Biological Sciences, Center for Systems Biology, University of Texas at Dallas, Richardson, TX 75080, USA

Abstract

Intratumor epigenetic heterogeneity is emerging as a key mechanism underlying tumor evolution and drug resistance. Epigenetic abnormalities frequently occur in medulloblastoma, the most common childhood malignant brain tumor. Medulloblastoma is classified into four subtypes including SHH medulloblastoma, which is characterized by elevated SHH signaling and a cerebellum granule neuron precursor (CGNP) cell-of-origin. Here we report that the histone H3K27 methyltransferase polycomb repressor complex 2 (PRC2) is often heterogeneous within individual SHH medulloblastoma tumors. In mouse models, complete deletion of the PRC2 core subunit EED inhibited medulloblastoma growth, while a mosaic deletion of EED significantly enhanced tumor growth. EED is intrinsically required for CGNP maintenance by inhibiting both neural differentiation and cell death. Complete deletion of EED led to CGNP depletion and reduced occurrence of medulloblastoma. Surprisingly, medulloblastomas with mosaic EED levels grew faster than control wildtype tumors and expressed increased levels of oncogenes such as *Igf2*, which is directly repressed by PRC2 and has been demonstrated to be both necessary and sufficient for SHH medulloblastoma progression. IGF2 mediated the oncogenic effects of PRC2 heterogeneity in tumor growth. Assessing clones of a human medulloblastoma cell line with different EED levels confirmed that EED^{low} cells can stimulate the growth of EED^{high} cells through paracrine IGF2 signaling. Thus, PRC2 heterogeneity plays an oncogenic role in medulloblastoma through both intrinsic growth competence and non-cell autonomous mechanisms in distinct tumor subclones.

Keywords

SHH medulloblastoma; PRC2; EED; tumor heterogeneity; IGF2; tumor subclone cooperation

[#]**Correspondence:** Jiang Wu, PhD, jiang9.wu@utsouthwestern.edu, Department of Physiology, UT Southwestern Medical Center, 5323 Harry Hines Blvd. Dallas TX 75390-9040, Phone: 214-648-1824.

Contributions

J.W. and J.Y. designed the experiments and analyzed the results. J.Y., B.K., X.S., and X.Z. performed the experiments and collected the data. Q.R.L. provided human medulloblastoma expression and prognosis data. Z.X. performed bioinformatics analyses. J.Y. and J.W. wrote the manuscript with the help from all authors.

Conflict of Interest:

The authors declare no potential conflicts of interest.

Introduction

Cancer development is driven by tumor-intrinsic mutations and is fueled by the tumor microenvironment (TME), which consists of various non-cancerous cells and cancer-derived subclones (1). Intratumor heterogeneity at the genetic or epigenetic levels is emerging as a widespread mechanism underlying tumor evolution and drug resistance (2). An important question is how different cancer subclones compete and cooperate. Non-cell autonomous mechanisms affecting neighboring cancer cells could underlie the oncogenic function of tumor heterogeneity (3). The significance of cancer subclone cooperation has been demonstrated in several cancer types. For example, in glioblastomas, cancer cells expressing a mutant EGFR stimulate the growth of cancer cells with a wild-type EGFR through cytokine secretion (4). In pediatric glioblastoma, inactivating mutations in the histone methyltransferase *KMT5B* confer increased invasion and migration on neighboring cells through chemokine signaling (5). Understanding the interactions between various cancer subclones could guide the development of new therapies.

Medulloblastomas, the most common childhood malignant brain tumor, are classified into four subgroups including WNT, SHH, Group 3, and Group 4 (6–10). Within these subgroups, SHH medulloblastomas are characterized by abnormally elevated Sonic hedgehog (SHH) signaling in cerebellum granule neuron precursors (CGNPs). During early postnatal development, CGNPs expand in a SHH-dependent manner and differentiate to granule neurons. A balanced CGNP proliferation and differentiation is precisely controlled by SHH signaling and additional factors. Abnormally elevated SHH signaling caused by various mutations leads to CGNP overexpansion and medulloblastoma. SHH medulloblastomas are highly heterogeneous at multiple levels including cytopathology, patient age, prognosis, and genomic and epigenetic abnormalities. The inter-tumor heterogeneity is believed to be caused by oncogenic pathways in addition to SHH signaling (11). Recent single-cell RNA-seq (scRNA-seq) studies further revealed intratumor heterogeneity in SHH medulloblastomas (12–14). SHH medulloblastomas contain mainly $ATOH1^+$ CGNP-like tumor propagating cells and $NEUROD1^+$ differentiated granule neurons. Other minor cell populations include $OLIG2^+$ cancer stem cells (12), other neuron subtypes, astrocytes, microglia (15), fibroblasts, immune cells (16), and blood vessel cells. Within single human medulloblastoma tumors, subclones that harbor different genetic mutations and recurrent potentials have been observed (17). However, it is not clear how these tumor subclones interact with each other and affect overall tumor growth.

Epigenetic regulators often play context-dependent roles in cancer development through the regulation of oncogenes or tumor suppressors in different cell types and at specific tumor developmental stages (18–21). One intriguing discovery from genomic studies of medulloblastoma is that there is a high rate of alterations of epigenetic regulators across all medulloblastoma subgroups (22). One dysregulated epigenetic pathway identified in medulloblastoma involves histone H3 lysine 27 trimethylation (H3K27me3) (10, 21, 23). The H3K27me3 methyltransferase PRC2 is a major transcription repressor. In many cancers, PRC2 displays oncogenic functions by repressing tumor suppressors or differentiation processes (24, 25), but PRC2 can also act as a tumor suppressor by repressing oncogenes

(24). The PRC2 core subunits EZH2/EZH1, EED, and SUZ12 are highly expressed in medulloblastoma with no loss-of-function mutations identified (23). It has been speculated that PRC2 is oncogenic in medulloblastoma (10). PRC2 inhibitors have been used to inhibit medulloblastoma growth in xenograft models (26, 27). However, a recent genetic study of Group 3 medulloblastoma showed an unexpected tumor-suppressor function of PRC2 (28). In addition, a study of PRC2 antibody staining of medulloblastoma tumor specimens showed that EZH2+ cell numbers vary from 20% to 80% among different tumors. The prognosis outcome is not simply associated with a higher or lower percentage of EZH2+ cells (29). Thus, PRC2 may play complex roles in medulloblastoma development.

In this study, we report that PRC2 heterogeneity drives medulloblastoma tumor growth. Whereas complete EED deletion leads to CGNP depletion and a reduced occurrence of medulloblastoma, medulloblastoma with mosaic EED levels grew faster than control wildtype tumors. We showed that PRC2-repressed IGF2 mediated the oncogenic effects of PRC2 heterogeneity. PRC2 heterogeneity controls medulloblastoma growth through both intrinsic growth competence and non-cell autonomous mechanisms in distinct tumor subclones.

Materials and Methods

Mice

The *Atoh1-Cre* mice (30) were provided by Dr. Lin Gan (Rochester University) and Dr. Jane Johnson (University of Texas Southwestern Medical Center). The $Atoh1^{+/-}$ mice (31) were provided by Dr. Helen Lai (University of Texas Southwestern Medical Center). The *TgAtoh1-Cre* mice (32), the *SmoM2* mice (33), the *CAG-CreER* mice (34), the *Ai9* reporter line (35), and the $Eed^{F/F}$ mice (36) were purchased from Jackson Laboratory. The $Eed^{F/F}$ mice contain *loxP* sites flanking exon 3–6 of the *Eed* gene. The NOD/SCID mice were purchased from the University of Texas Southwestern Mouse Breeding Core Facility. All mice are maintained on a mixed genetic background at the University of Texas Southwestern Medical Center Animal Facility. Both males and female mice were used for analyses at the indicated ages with no significant differences between them. All animal procedures were approved by IACUC and performed in accordance with the IACUC animal use guidelines.

Immunostaining, image processing and BrdU tracing

Paraffin sections of brain or tumor tissues were used for hematoxylin and eosin (H&E) staining as well as immunostaining. For the proliferation assay, BrdU (100 mg/kg; B5002; Sigma-Aldrich) was injected intraperitoneally (adult) or subcutaneously (neonatal) 30 minutes before harvesting. For cell lineage tracing, BrdU (100 mg/kg; B5002; Sigma-Aldrich) was injected subcutaneously in neonatal pups 24 hours before harvesting. The antibodies used for IHC were against Ki67 (SolA15, # 14–5698-82, eBioscience), BrdU (G3G4, DSHB), GFAP (#556330, BD Biosciences), HuC/D (#ab184267, Abcam), H3K27me3 (#07–449, Millipore), RFP (#600–401–379, Rockland), NEUROD2 (#ab104430, Abcam), NeuN (#ABN78, Millipore), cleaved Caspase 3 (#9664, Cell Signaling Technology), EED (#85322, Cell Signaling Technology), CRE (#15036, Cell Signaling Technology), and PAX6 (PAX6, DSHB). For IHC staining, biotinylated

goat anti-rabbit (#BA-1000, Vector Laboratories) or goat anti-mouse (#BA-9200, Vector Laboratories) secondary antibodies were used. The counterstain used was either hematoxylin (#H-3401, Vector Laboratories) or methyl green (#H-3402, Vector Laboratories). For immunofluorescent staining, Alexa 488 conjugated goat anti-rabbit (Thermo Fisher Scientific Cat# A-11008, RRID:AB_143165) and Alexa 594 conjugated goat anti-mouse (Thermo Fisher Scientific Cat# A-11032, RRID:AB_2534091) secondary antibodies were used. For the EED and CRE IHC co-stain, three consecutive sections were used to stain EED, CRE, and EED/CRE. The co-stain of EED and CRE was performed following the protocol IHC Multiplexing Guide from VECTOR Laboratories. Bright-field images were acquired using a Hamamatsu Nanozoomer 2.0 HT whole slide scanner at the University of Texas Southwestern Medical Center Whole Brain Microscopy Facility. Fluorescent images were acquired by a confocal system (Zeiss LSM710). Quantifications were performed blindly by counting positive cells from three images per tumor and processed using ImageJ (RRID:SCR_003070). At least three biological replicates were used in each experiment.

Tumor transplantation

Medulloblastoma spontaneously grown from *CAG-CreER SmoM2 Eed*$^{F/F}$ mice were dissected and dissociated. The tumor cells (5×10^6) were mixed with Matrigel (BD Biosciences) and injected subcutaneously in the flank regions of 6-week-old NOD/ SCID mice. One day after tumor injection, mice were injected intraperitoneally with oil solvent or one or 10 doses of tamoxifen (75 mg/kg) every other day during a 20-day period before being sacrificed for tumor analyses.

Flow cytometry

Medulloblastomas were dissected and dissociated. Cells were fixed and permeabilized in 4% PFA with 0.1% saponin (Sigma-Aldrich 47036) for 30 min at 4 °C. The primary antibodies used were against EED (Cell Signaling Technology Cat# 85322,) and CRE (Cell Signaling Technology Cat# 15036, RRID:AB_2798694). The secondary antibody used was anti-rabbit IgG-PE (#111-116-144, Jackson Immunoresearch Laboratory). Stained cells were analyzed with a BD FACSCalibur machine (BD Bioscience). The Flowjo software (RRID:SCR_008520) was used for data analyses.

Chromatin immunoprecipitation (ChIP)

The ChIP experiments were performed as described previously (37). Dounced tumors were crosslinked with 1% PFA and sonicated into fragments. The antibodies used were against H3K27me3 (Millipore Cat# 07–449, RRID:AB_310624) and EED (Cell Signaling Technology Cat# 85322). The precipitated DNA was purified and subjected to real-time PCR. The graphics shown are representative of experiments performed in triplicate. The experiments were repeated three times.

RT-PCR, qPCR, and genotyping PCR

The RNA from Daoy cells or tumor tissues was extracted with TRIZOL (Invitrogen). cDNAs were synthesized by reverse transcription using Iscript (Bio-Rad), followed by PCR or quantitative PCR analysis. A Bio-Rad real-time PCR system (C1000 Thermal Cycler) was

used for quantitative PCR. *GAPDH* was used to normalize input RNA. The PCR primer sequences were listed in Table S1. Genomic DNA for genotyping was isolated from tails or tumor tissues using a PBND (PCR buffer with nonionic detergents) preparation. A Bio-Rad C1000 Thermal Cycler was used for PCR. The PCR primer sequences were listed in Table S1.

RNA-seq analyses

For RNA-seq, total RNAs were extracted, followed by library preparation, using the Illumina RNA-Seq Preparation Kit and sequencing on a HiSeq 2500 sequencer at the University of Texas Southwestern Sequencing Core Facility. The expression levels of genes were quantified by a Kallisto program (38), and the differentially expressed genes were detected by an EdgeR program (RRID:SCR_012802) (39). Genes with a count-per-million (CPM) of less than 1 in more than 2 samples were excluded. The differentially expressed genes with a fold change larger than 2 and an FDR<0.05 were selected as EED-regulated genes. Gene ontology analysis was performed using DAVID tools (RRID:SCR_001881, http://david.abcc.ncifcrf.gov/).

Analyses of human medulloblastoma expression data

The gene expression data from subtype classified human medulloblastoma were extracted from previous studies (11, 40). The Kaplan-Meier method was used to compare the survival probability of patients with different tumor expressions of PRC2 subunits (40). Single cell Smart-seq expression data were extracted from a previous study (13). The expression of candidate genes in all ATOH1+ cells were analyzed.

Cell cultures

The medulloblastoma cell line Daoy was purchased from ATCC (HTB-186) and was cultured as suggested by the supplier. It tested negative for mycoplasma using MycoAlert Mycoplasma Detection Kit (Lonza, USA). Cells between 4–6 passages were used in the study. Conditioned media were collected from Daoy cultures 24 hours after changing to the serum free medium and were used to culture EED^{wt} Daoy cells for 72 hours before measuring cell viability. For co-culture experiments, EED^{wt}, EED^{ko}, or mixed (4 EED^{wt}:1 EED^{ko}) cells were seeded in 96-well plate at 5,000 cells per well. After culturing for 24 hours in complete media (containing 10% FBS), culture media were changed to serum free media or serum free media with 2 ug/ml IGF2 antibody (R&D Systems Cat# AF-292-NA, RRID:AB_354449) for another 72 hours, or 200 ng/ml recombinant human IGF2 (#292-G2, R&D Systems) for 24 hours before measuring cell viability. Relative cell titer was determined using the CellTiter-Glo® Luminescent Cell Viability Assay (Promega, #G7572) according to the manufacture's instruction. For inhibitor experiments, GSK-126 (#S7061, Selleckchem) was added to culture media for 72 hours before measuring gene expression.

Lentivirus preparation and infection

For packaging the lentivirus, CRISPR-cas9-based guide RNA (gRNA) targeting human *EED* (GATCATAACCAACCATTGTT) was cloned in LentiCRISPR v2 (Addgene 52961), which was mixed with psPAX2 (RRID:Addgene_12260) and pMD2.G (Addgene #12259)

and transfected into HEK 293T cells (ATCC, # CRL-3216) using Polyjet (Signagen). Supernatant containing the viruses was collected 48–72 hours after transfection and used for subsequent infection. Daoy cells were infected with lentiviral supernatant containing 8 ug/ml polybrene for 24 hours. In order to select EED^{ko} Daoy cells, puromycin (1 μg/ml) was added three days after initial infection for one week. Single cell clones were selected by limiting dilution. EED deletion was confirmed by immunofluorescent staining.

Immunoblotting

Daoy cells or tumor tissues were lysed in RIPA buffer (50 mM Tris, pH 8, 250 mM NaCl, 0.05% SDS, 0.5% DOC, 1% NP-40) in the presence of phosphatase inhibitors. The cell lysates were separated on 12% SDS-PAGE gels. The antibodies used were against IGF2 (# MA5–17096, Invitrogen), AKT (#sc-8312, Santa Cruz Biotechnology) and p-AKT (#4060, Cell Signaling Technology).

Statistical analysis

The data are expressed as means ± s.d. All experiments were repeated for 3 times unless otherwise indicated. Statistical analysis was performed by either an ANOVA post hoc t-test for multiple comparisons or a two-tailed unpaired Student's t-test. For the morbidity studies, the Kaplan-Meier method was used to plot the survival curve, and the log-rank test was used for statistical analyses. A p-value < 0.05 was considered significant.

Data availability

RNA sequencing data have been deposited in the Gene Expression Omnibus (GEO). The accession number is GSE206009.

Results

EED is required for normal mouse cerebellar development

SHH medulloblastoma is caused by abnormally active SHH signaling in CGNPs. To determine the function of PRC2 in CGNPs and medulloblastomas, we deleted the PRC2 core subunit-encoding *Eed* gene specifically in CGNPs using a knock-in pan CGNP *Atoh1-Cre* driver (30) (Figure S1A). EED deletion results in the degradation of other PRC2 subunits and loss of PRC2 function (36). Atoh1-Cre-mediated *Eed* deletion led to severe ataxia and reduced body weight in mutant mice (supplemental video and Figure S1B). In mature cerebella at postnatal day 28 (P28), H&E and NeuN staining showed that *Eed* deletion caused close-to-complete depletion of granule neurons without significantly altering cerebellar foliation (Figure 1A). In *Eed*-deleted cerebella during development at P7, EED protein deletion and a decrease in H3K27me3 were prominent in most CGNPs, which were identified as PAX6+ cells in the external granule layer (EGL) (41) (Figure 1B, 1C). We observed a gradual decrease in thickness of the EGL, where CGNPs reside, from P2 to P7, indicating an early depletion of CGNPs (Figure S1C).

We then examined the function of PRC2 in CGNP proliferation and differentiation. Using BrdU pulse labeling (30 min) at P2, we did not observe a significant difference between the percentage of BrdU+ cells in control and in *Eed*-deleted EGLs (Figure 1D). Staining

the mitotic marker Ser10-phosphorylated histone 3 (H3P) also showed similar levels in the EGLs of control and *Eed*-deleted cerebella (Figure S1D). These results suggest that EED does not directly affect CGNP proliferation rate. We previously showed that a proneural gene *NeuroD2* is activated by H3K27me3 demethylase UTX and promotes granule neuron differentiation (16). Antibody staining of P7 cerebella showed that NEUROD2 starts to express in differentiating granule neurons in the inner EGL and increases in level as differentiated granule neurons migrate to the inner granule layer (IGL) and mature. Compared to controls, there was a significant increase of NEUROD2 staining in *Eed*-deleted CGNPs in EGL (Figure 1E). In a BrdU tracing experiment, in which pups at P1 were injected with BrdU 24 h before examination, the newly differentiated neurons were co-labeled with BrdU and a neuronal marker HuC/D. The percentage of BrdU+ HuC/D+ cells within all BrdU+ cells was significantly higher in *Eed*-deleted EGLs (Figure 1F, 1G), confirming enhanced neuronal differentiation upon EED deletion. Next, we observed increased active caspase 3 staining in EGLs, indicating an increase of cell death in *Eed*-deleted CGNPs compared to controls (Figure 1H). In addition, we observed a significant increase in GFAP staining in *Eed*-deleted P7 cerebella (Figure 1I). The radial shaped GFAP signals in the molecular layer (ML) extending to EGL reflect Bergmann glia, which was significantly increased in the *Atoh1-Cre Eed*$^{F/F}$ cerebellum. The increased GFAP signals suggest reactive Bergmann glia cells in response to the CGNP abnormalities induced by EED deletion. Together, EED deletion led to close-to-complete CGNP and granule neuron depletion. EED is required for normal granule neuron differentiation and survival in the cerebellum.

EED is important for SHH medulloblastoma formation

In a well-characterized SHH medulloblastoma mouse model, which was caused by a Cre-induced constitutively active *SmoM2* mutation (33), we deleted *Eed* from precancerous CGNPs using *Atoh1-Cre*. Deletion of *Eed* from medulloblastoma mice also caused CGNP depletion and severe ataxia. As a result, compared to the 100% medulloblastoma occurrence in *SmoM2* mice with wild-type *Eed*, EED deletion reduced cancer occurrence rate to only about 35% (Figure 2A). The *Eed*-deleted tumors were generally small and EED negative. They were less dense and showed lower proliferation rates by Ki67 staining (Figure 2B). SHH medulloblastoma mainly consists of CGNP-like cancer cells and differentiated granule neurons, both of which express PAX6. Tumor CGNPs can also differentiate to GFAP+ astrocytes (15). Although both control and *Eed*-deleted tumors consisted mostly of PAX6+ cells, *Eed*-deleted tumors displayed decreased PAX6 levels and less granule neurons (PAX6+, HuC/D+) (Figure 2C). We also observed a significant increase of GFAP expression in *Eed*-deleted tumors (Figure 2D). It remains unclear whether and how these changes affected tumor survival without EED. Thus, EED is important for progenitor and tumor development in SHH medulloblastoma, likely in a cell-autonomous manner.

Heterogeneous TgAtoh1-Cre activity led to incomplete EED deletion and mild cerebellar defects

Using another well-characterized CGNP-specific transgenic *Atoh1-Cre* line (*TgAtoh1-Cre*) (41), we observed an unexpectedly mild phenotype in *Eed*-mutant cerebella. *TgAtoh1-Cre Eed*$^{F/F}$ mice were viable and did not show obvious motor defects. Anatomically, we only

observed minor changes in mutant cerebella at P28, in which the granule neurons in the IGL were less dense than those in control cerebella (Figure 3A). This defect in granule neuron loss was more obvious in the anterior lobes than in the posterior lobes. In developing cerebella at P7, we observed various levels of EED deletion in the *TgAtoh1-Cre Eed*$^{F/F}$ EGL as shown by antibody staining. More EED-deleted CGNPs were observed in anterior lobes than in posterior regions (Figure 3B). Similar to the EED-deleted *Atoh1-Cre Eed*$^{F/F}$ cerebella, the anterior EGL regions of *TgAtoh1-Cre Eed*$^{F/F}$ mice at P7 displayed increased NEUROD2 expression and increased caspase 3 staining than control mice (Figure 3C), confirming a function of EED in preventing abnormal CGNP differentiation and cell death.

The incomplete deletion of EED led us to re-examine the TgAtoh1-Cre expression and activities. Although high levels of Cre proteins were detected throughout the EGLs in P5 cerebella, their levels were heterogeneous. Cre levels were relatively high in some anterior EGL regions, but were more mosaic in other regions (Figure 3D). The Cre activities were examined using the *Ai9* reporter line that contains an *R26R-floxed stop-tdTomato* allele (35). Interestingly, TgAtoh1-Cre-mediated recombination led to the expression of tdTomato in almost all CGNPs in EGL at P5 (Figure 3D), which is consistent with previous observations that the *TgAhoh1-Cre* allele is widely active in CGNPs (41). Together, these results indicate that there were heterogeneous levels of Cre proteins and activities in *TgAtoh1-Cre* CGNPs, which we termed Cre^{high} and Cre^{low}. In *TgAtoh1-Cre Ai9* mice, the Cre activities in both Cre^{high} and Cre^{low} CGNPs were sufficient to recombine the "easy" *R26R-floxed stop-tdTomato* locus. However, in *TgAtoh1-Cre Eed*$^{F/F}$ mice, while Cre^{high} CGNPs could effectively delete *Eed*, low Cre activities in Cre^{low} CGNPs failed to completely recombine the more "difficult" *Eed*^{F} allele before CGNPs differentiate to granule neurons, resulting in a mosaic deletion of EED in CGNPs and mild cerebellum defects.

Besides the Cre activities, the other difference between the *Atoh1-Cre* and *TgAtoh1-Cre* is that the knock-in *Atoh1-Cre* led to *Atoh1* heterozygosity, whereas *TgAtoh1-Cre* mice has two wildtype *Atoh1* copies. To determine whether *Atoh1* dosage could contribute to the different patterns of EED deletion in these two Cre mice, we generated the *TgAtoh1-Cre Atoh1*$^{+/-}$ *Eed*$^{F/F}$ mice (31) (Figure S2A). Although losing one copy of *Atoh1* from the *TgAtoh1-Cre Eed*$^{F/F}$ mice led to a more severe loss of granule neurons in P28 cerebella, many neurons in the posterior lobes remain (Figure S2B). EED staining also showed mosaic EED deletion in *TgAtoh1-Cre Atoh1*$^{+/-}$ *Eed*$^{F/F}$ CGNPs in P8 EGLs (Figure S2C). Thus, the incomplete EED deletion in *TgAtoh1-Cre Eed*$^{F/F}$ CGNPs was mostly caused by the heterogeneous *TgAtoh1-Cre* activities.

TgAtoh1-Cre SmoM2 Eed$^{F/F}$ mice showed enhanced tumor growth with mosaic EED deletion

Strikingly, in contrast to the depletion of CGNPs and reduced tumor occurrence after complete EED deletion in the *Atoh1-Cre SmoM2 Eed*$^{F/F}$ mice, the *TgAtoh1-Cre SmoM2 Eed*$^{F/F}$ mice had enhanced tumor growth and shortened survival time compared to control wildtype and *Eed*$^{F/+}$ tumor mice. Compared to a 38-day median survival time for *TgAtoh1-Cre SmoM2 Eed*$^{+/+}$ mice, *TgAtoh1-Cre SmoM2 Eed*$^{F/F}$ mice had only a 23-day median survival time with aggressive tumor growth (Figure 4A, 4B). Compared to wildtype tumors,

Eed$^{F/F}$ tumors had increased proliferation rates as shown by BrdU labeling (Figure 4C) and decreased cell death rate as shown by active caspase 3 staining (Figure 4D). Deleting one copy of *Atoh1* from the *TgAtoh1-Cre SmoM2* mice delayed the tumor occurrence and progression for all three *Eed* genotypes. The survival times were still significantly shortened in *Eed*$^{F/F}$ mice compared to *Eed*$^{+/+}$ and *Eed*$^{F/+}$ mice (Figure S2D). These results suggest an unexpected tumor suppressor function of PRC2 in SHH medulloblastoma.

We then examined EED and Cre protein expression in the *TgAtoh1-Cre SmoM2* tumors. In *Eed*$^{+/+}$ tumors, both EED levels and Cre levels were high in most tumor cells, as expected. There were also some variations in EED and Cre levels, which reflects the different cell types in the tumor as well as the heterogeneous TgAtoh1-Cre expression pattern (Figure 4E). A more quantitative measurement using FACS showed that in wildtype tumors, more than 85% of cells were EED^{high} and more than 65% were Cre^{high} cells (Figure 4F, 4G). Interestingly, in *Eed*$^{F/F}$ mutant medulloblastomas, many cells still expressed EED (Figure 4E). FACS analyses showed that in *Eed*$^{F/F}$ medulloblastomas, ~68% of the cells retained EED. The EED^{low} cells were increased in *Eed*$^{F/F}$ tumors than in *Eed*$^{+/+}$ tumors, but they only consisted of ~32% of all *Eed*$^{F/F}$ tumor cells (Figure 4F). Intriguingly, in *Eed*$^{F/F}$ medulloblastomas, Cre^{high} cells were significantly reduced to ~15% (Figure 4E, 4G). Therefore, in *TgAtoh1-Cre* induced medulloblastomas, Cre^{low} cells are likely a minor population but are disproportionally expanded in *Eed*$^{F/F}$ mutant medulloblastomas, contributing to overall faster tumor growth. The Cre^{low} population likely retained one wildtype *Eed* allele, as confirmed by co-staining and genotyping (Figure 4E, 4H). In these *Eed*$^{F/F}$ mutant medulloblastoma, there are subclones of tumor cells with different Cre activities and EED levels (Cre^{high} EED^{low} and Cre^{low} EED^{high}). The EED deletion in Cre^{high} EED^{low} subclones may lead to the overexpansion of the Cre^{low} EED^{high} population and faster overall tumor growth.

Igf2 is a PRC2 target that was derepressed in *TgAtoh1-Cre SmoM2 Eed*$^{F/F}$ tumors

To identify EED-regulated genes and pathways involved in promoting mosaic medulloblastoma growth, we performed RNA-seq and compared transcriptomes of the *TgAtoh1-Cre SmoM2 Eed*$^{+/+}$ medulloblastomas with those of the mosaic *TgAtoh1-Cre SmoM2 Eed*$^{F/F}$ tumors (Figure 5A). The results showed that few genes involved in the core SHH pathway or in the neural developmental process were changed significantly (Figure S3). The level of key SHH medulloblastoma signature genes such as *Gli1*, *Atoh1*, and *NeuroD1* were similar between *Eed*$^{+/+}$ and *Eed*$^{F/F}$ tumors, indicating that the fast growth of *Eed*$^{F/F}$ medulloblastomas was likely not due to changes in the tumor cell-intrinsic fate. The cancer stem cell markers *Olig2* and *CD133*, as well as the recently identified glia/microglia/Igf1 TME pathway genes (15), were also not changed (Figure S3). Of the 231 upregulated genes in the *Eed*$^{F/F}$ mutant medulloblastoma (fold change >2, $p<0.05$), many are classical PRC2 targets such as *Hox* gene clusters, muscle development genes, and tumor suppressors such as *Cdkn1c* (Figure 5A, 5B, S3). Notably, some of the upregulated genes in *Eed*$^{F/F}$ mutant medulloblastomas encode oncogenic molecules such as IGF2, NOTCH1, and LIN28b (Figure 5A–B). Using RT-qPCR, we confirmed that *Igf2* was increased in *TgAtoh1-Cre SmoM2* medulloblastoma when *Eed* was deleted for one or both copies (Figure 5C). IGF2 proteins in tumors were also increased upon EED deletion (Figure 5D). We performed

H3K27me3 ChIP-seq of *SmoM2* medulloblastoma and observed extensive H3K27me3 signals around the EED-repressed oncogenes including *Igf2* (Figure 5E). Using ChIP-qPCR, we showed that EED directly binds to the *Igf2* promoter (Figure 5F). Upon EED deletion in the $Eed^{F/F}$ medulloblastomas, EED binding as well as local H3K27me3 levels were reduced (Figure 5G). The main signaling pathway downstream of IGF2 is the PI3K/AKT pathway, and high levels of phosphorylated AKT (p-AKT) were observed in some SHH medulloblastoma patients with poor prognoses (11). Indeed, we observed increased p-AKT levels in $Eed^{F/F}$ mutant medulloblastomas compared to wild-type medulloblastomas (Figure 5H). Thus, *Igf2* is a PRC2 target that was derepressed in *TgAtoh1-Cre SmoM2* $Eed^{F/F}$ tumors.

Second mouse model demonstrating the oncogenic function of PRC2 heterogeneity

We showed that a mosaic deletion of EED led to faster tumor growth. To exclude the possibility of unknown effects of the expression of TgAtoh1-Cre, we induced mosaic EED deletion in SHH medulloblastoma in another mouse model. Previously, we developed a genetic system able to delete specific genes in medulloblastoma after tumor formation (20). *CAG-CreER SmoM2* $Eed^{F/F}$ mice develop SHH medulloblastoma spontaneously (33). Basal Cre activities could induce *SmoM2* at the *Rosa26* locus but are not sufficient to delete *Eed*. *Eed* could then be deleted by tamoxifen induction in a dose-dependent manner. We transplanted the *CAG-CreER SmoM2* $Eed^{F/F}$ medulloblastomas subcutaneously to NOD/SCID mice, which were then injected with tamoxifen or an oil control (Figure 6A). The transplanted tumor cells with control oil injection were EED^{high} (Figure 6B, 6C). When tamoxifen was injected 10 times (10xTAM) post transplantation, EED was mostly deleted from the tumor cells, and tumor growth was significantly inhibited (Figure 6B, 6C). On the contrary, injecting tamoxifen only once (1xTAM), which partially deleted EED in transplanted tumors, resulted in enhanced tumor growth (Figure 6B, 6C). In EED heterogeneous tumors, *Igf2* expression level was increased compared to the oil-treated homogeneous EED^{high} tumors (Figure 6D). Thus, using a second genetic system, we confirmed that while a complete EED deletion led to tumor inhibition, a mosaic EED deletion promoted medulloblastoma growth, possibly through the increased IGF2 signaling.

PRC2 heterogeneity and IGF2 expression in human medulloblastoma samples

IGF2 is especially of interest to SHH medulloblastoma research because it is specifically expressed at high levels in human SHH medulloblastomas compared to other medulloblastoma types, based on the analysis of a cohort of 172 medulloblastoma patients (40) (Figure 7A). Previous genetic studies also showed that IGF2 or its receptor IGF1R is necessary and sufficient for promoting SHH medulloblastoma progression in mice (15, 42, 43). Our results suggest that the *Igf2* gene is directly repressed by PRC2 in SHH medulloblastoma. Thus, IGF2 could be a key signaling molecule that is derepressed in EED^{low} cells and stimulates the growth of EED^{high} cells. After analyzing a previously published SHH medulloblastoma microarray data set (44), we also observed an overall increase in *IGF2* expression levels in SHH medulloblastomas with lower *EED* levels compared to the group with higher *EED* levels (Figure 7B).

PRC2 subunits are highly expressed in all 4 medulloblastoma subgroups (Figure 7C). When separated by tumor PRC2 subunit expression levels, a prognosis analysis of the SHH medulloblastoma patients showed that relatively low levels of both *EED* and *SUZ12* correlated with worse prognosis outcomes (Figure 7D). These results suggest that PRC2 has a tumor suppressor function in addition to its potential oncogenic function in SHH medulloblastoma. To further determine whether PRC2 heterogeneity could underly the seemingly paradoxical functions of PRC2 in SHH medulloblastoma, we analyzed PRC2 subunit expression in SHH medulloblastoma at single cell levels. A recent single cell study of human medulloblastomas (13), which used the Smart-seq protocol that has better sequencing depth, enabled us to examine PRC2 subunit levels in single cells. In all three available SHH medulloblastoma samples representing three subtypes that occur in infants, children, and adults, respectively, PRC2 subunits displayed heterogeneous levels from high to undetectable for all 4 subunits in ATOH1+ CGNP-like cancer-propagating cells (Figure 7E). About 10–30% of ATOH1+ cells had no detectable levels of PRC2 subunits in these SHH medulloblastoma samples. PRC2 heterogeneity had no correlation with levels of the SHH medulloblastoma marker GLI2. Interestingly, higher PRC2 levels in single medulloblastoma cells appeared to correlate with higher levels of the proliferation marker MKI67 (Figure 7E). $PRC2^{high}$ medulloblastoma cells could have a higher proliferation rate than $PRC2^{low}$ medulloblastoma cells. On the contrary, the presence of the slow-proliferating $PRC2^{low}$ tumor cells suggests that they also contribute to the growth of the tumor. Thus, PRC2 heterogeneity is common in human SHH medulloblastoma. Our mouse genetic experiments and human medulloblastoma analyses together support a model in which PRC2 heterogeneity drives tumor growth. In a heterogeneous tumor that contains both $PRC2^{high}$ and $PRC2^{low}$ cells, the $PRC2^{low}$ subclones, despite having a lower growth competence, enhance $PRC2^{high}$ subclone growth through non-cell autonomous mechanisms such as IGF2 signaling. The overall enhanced tumor growth is a result of the cooperation between $PRC2^{high}$ and $PRC2^{low}$ cancer cells (Figure 7F).

An IGF2/PI3K/AKT pathway mediated non-cell autonomous tumor suppressor function of PRC2 in human medulloblastoma Daoy cells

Using the human SHH medulloblastoma cell line Daoy (45), we further investigated the potential IGF2 mediated non-cell autonomous tumor suppressor function of PRC2. We first confirmed that *IGF2* is repressed by PRC2 in Daoy cells. Treating Daoy cultures with the PRC2 enzymatic inhibitor GSK-126 led to increased *IGF2* expression in a dose-dependent manner as shown by RT-qPCR (Figure 8A). Using the CRISPR-Cas9 method, we generated several EED^{ko} Daoy clones (Figure 8B). An RNA-seq analysis comparing EED^{wt} and EED^{ko} Daoy clones (n=2) also showed the increased expression of oncogenes including *IGF2* and *NOTCH1/HES1* (Figure 8C). Interestingly, many EED-reregulated genes encode extracellular factors (Figure 8D, Table S2), which could support a role of PRC2 in regulating tumor growth via non-cell autonomous mechanisms. Using RT-qPCR, we confirmed the increase of *IGF2* expression in EED^{ko} Daoy clones compared to the control EED^{wt} clones (Figure 8E). Our data showed that EED^{ko} cells have similar or slower growth rates compared to EED^{wt} controls (Figure 8F). Interestingly, a 4:1 mix of EED^{wt} and EED^{ko} cells led to increased growth rates compared to the growth rates of EED^{wt} and EED^{ko} cells cultured separately (Figure 8F). In addition, the conditioned media

collected from *EED*^{ko} cells enhanced *EED*^{wt} Daoy cell growth more than did the media collected from the control *EED*^{wt} cells (Figure 8G). Consistent with the role of the IGF2/PI3K/AKT pathway in mediating the non-cell autonomous function of PRC2 in tumor cell growth, conditioned media from the *EED*^{ko} cells caused increased AKT phosphorylation in cultures compared to the addition of *EED*^{wt} media (Figure 8H). These results showed that, similar to our observation in mouse SHH medulloblastomas, PRC2 heterogeneity in a human SHH medulloblastoma cell line led to increased growth, possibly through increased IGF2 production from the *EED*^{ko} clones.

To determine whether IGF2 is a key PRC2 target mediating the enhanced growth of Daoy cells with heterogeneous levels of PRC2, we applied neutralizing IGF2 antibodies to the mixed culture of *EED*^{wt} and *EED*^{ko} cells. The enhanced growth of the mixed culture diminished upon blocking IGF2 signaling (Figure 8I). On the contrary, adding recombinant IGF2 in the media significantly increased growth of Daoy cells (Figure 8J), possibly by increased IGF2/PI3K/AKT pathway activity (Figure 8K). Together, our data reveal a novel oncogenic pathway in SHH medulloblastomas driven by PRC2 heterogeneity through derepressed IGF2 signaling and the downstream PI3K/AKT pathway.

Discussion

In this study, we report that PRC2 heterogeneity drives medulloblastoma tumor growth by its intrinsic oncogenic function and a novel non-cell autonomous tumor suppressor function (Figure 7F). We revealed that the PRC2 repressed IGF2/PI3K/AKT pathway plays a key role in mediating the non-cell autonomous function of PRC2. Thus, we uncovered a novel mechanism underlying the oncogenic functions of tumor epigenetic heterogeneity during tumor evolution.

Several pieces of evidence support a novel oncogenic mechanism arising from PRC2 heterogeneity in cancer subclones. Firstly, we generated two mouse medulloblastoma models that contain PRC2^{high} and PRC2^{low} cancer cells. Both mosaic models demonstrated significantly enhanced growth compared to homogeneous tumors (Figure 4, 6). Secondly, we generated *EED*^{wt} and *EED*^{ko} clones of the human medulloblastoma cell line Daoy. Using mixed cultures or conditioned media culture, we showed that *EED*^{ko} clones could stimulate the growth of *EED*^{wt} clones (Figure 8). Thirdly, we identified EED-repressed IGF2 as a secreted oncogenic factor, which could mediate the non-cell autonomous function of PRC2. Finally, we showed that PRC2 heterogeneity is common in human SHH medulloblastoma. Subclones with different PRC2 levels appear to have different proliferation competence (Figure 7E).

During tumor development, PRC2 heterogeneity could be generated through several mechanisms. Firstly, cancer cells at distinct differentiation stages may form heterogeneous subclones. In small-cell lung cancer, where the activation of the Notch pathway results in a neuroendocrine to non-neuroendocrine fate switch in 10–50% of tumor cells (46). The slow growing non-neuroendocrine cells could provide trophic support to neuroendocrine tumor cells. In medulloblastoma, PRC2 levels are high in stem cell-like cancer cells and are decreased upon differentiation. Although we observed abnormal differentiation upon PRC2

deletion in CGNPs, it remains unclear how it plays a role in tumor growth. Secondly, genetic mutations in specific cancer subclones could generate tumor heterogeneity. In pediatric glioblastoma, inactivating mutations in *KMT5B* were only present in <1% of tumor cells but conferred increased invasion and migration on neighboring cells (5). To date, PRC2 mutation has not been identified in medulloblastoma. A targeted deep sequencing may reveal possible PRC2 mutations. Finally, PRC2 heterogeneity could be achieved by epigenetic suppression. An examination of the epigenetic states of PRC2 subunit genes at single tumor cell levels may reveal the potential mechanisms underlying PRC2 heterogeneity.

During tumor evolution, the presence of non-cell autonomous effects between subclones not only brings new tumor phenotypes, but also maintains sub-clonal heterogeneity (47). Subclone competition and cooperation could stabilize sub-clonal heterogeneity, as was shown in mixed xenograft models of different breast cancer clones expressing trophic factors (3). In the *TgAtoh1-Cre EED*$^{F/F}$ mouse medulloblastoma model, mosaic Cre activities led to unsynchronized deletion of EED. EED^{high} cells have high growth competence. The accumulation of Cre activities in tumor cells would continue to turn EED^{high} cells to EED^{low} cells, which in turn support EED^{high} cells. The overexpansion of EED^{high} cells and the turnover from EED^{high} to EED^{low} cells may reach a balance during tumor development. In human tumors, we speculate that the PRC2^{low} clones may arise by epigenetic repression, copy loss, or rare mutations. The PRC2^{low} subclones grow more slowly and represent a smaller portion of the heterogenous tumor. However, PRC2^{low} subclones would not be completely lost due to their non-cell autonomous supportive function required for the overall tumor growth. Subclone competition and cooperation could stabilize the PRC2 heterogeneity in tumors.

In addition to IGF2, we also identified additional candidate PRC2-repressed oncogenes such as *NOTCH1/HES1* and *LIN28b* (Table S2, Figure 5A, 8C). Interestingly, both *NOTCH1* and *LIN28b* have been shown to have non-cell autonomous oncogenic functions. Overexpression of NOTCH1 in cerebellum progenitors in the absence of p53 led to the development of SHH medulloblastoma in mice. The oncogenic function appears to be non-cell autonomous since NOTCH1 was only overexpressed in a small number of tumor cells (48). *LIN28b* is an oncogene that is highly expressed in SHH medulloblastoma. Interestingly, LIN28b also could function non-cell autonomously by promoting IGF2 protein levels (49). Thus, these oncogenes may contribute to the oncogenic function of PRC2 heterogeneity.

PRC2 plays context-dependent roles in cancer development with both oncogenic and tumor suppressor functions. In medulloblastoma, the pleiotropic functions of PRC2 in cooperative cancer subclones underlie the oncogenic function of PRC2 heterogeneity, which may occur in many other cancer types and may guide the development of new therapeutic strategies.

Supplementary Material

Refer to Web version on PubMed Central for supplementary material.

Acknowledgements

We are grateful to Drs. Jane Johnson and Lin Gan for providing the *Atoh1-Cre* mice and Dr. Helen Lai for providing *the Atoh1*$^{+/-}$ mice. We thank Dr. Zaili Luo for assisting the human medulloblastoma expression data analyses. We thank Dr. Xiaoye Liu and Huaxia Dong for technical help, and Michael Zhan for editing the manuscript. This work was supported by grants from NIH (R01NS096068 and R21NS127401 to J. Wu) and CPRIT (RP220235 to J. Wu).

References

1. Hanahan D Hallmarks of Cancer: New Dimensions. Cancer discovery. 2022;12:31–46. [PubMed: 35022204]
2. Mazor T, Pankov A, Song JS, Costello JF. Intratumoral Heterogeneity of the Epigenome. Cancer Cell. 2016;29:440–51. [PubMed: 27070699]
3. Marusyk A, Tabassum DP, Altrock PM, Almendro V, Michor F, Polyak K. Non-cell-autonomous driving of tumour growth supports sub-clonal heterogeneity. Nature. 2014;514:54–8. [PubMed: 25079331]
4. Inda MM, Bonavia R, Mukasa A, Narita Y, Sah DW, Vandenberg S, et al. Tumor heterogeneity is an active process maintained by a mutant EGFR-induced cytokine circuit in glioblastoma. Genes Dev. 2010;24:1731–45. [PubMed: 20713517]
5. Vinci M, Burford A, Molinari V, Kessler K, Popov S, Clarke M, et al. Functional diversity and cooperativity between subclonal populations of pediatric glioblastoma and diffuse intrinsic pontine glioma cells. Nat Med. 2018;24:1204–15. [PubMed: 29967352]
6. Jones DT, Jager N, Kool M, Zichner T, Hutter B, Sultan M, et al. Dissecting the genomic complexity underlying medulloblastoma. Nature. 2012;488:100–5. [PubMed: 22832583]
7. Northcott PA, Shih DJ, Peacock J, Garzia L, Morrissy AS, Zichner T, et al. Subgroup-specific structural variation across 1,000 medulloblastoma genomes. Nature. 2012;488:49–56. [PubMed: 22832581]
8. Parsons DW, Li M, Zhang X, Jones S, Leary RJ, Lin JC, et al. The genetic landscape of the childhood cancer medulloblastoma. Science. 2011;331:435–9. [PubMed: 21163964]
9. Pugh TJ, Weeraratne SD, Archer TC, Pomeranz Krummel DA, Auclair D, Bochicchio J, et al. Medulloblastoma exome sequencing uncovers subtype-specific somatic mutations. Nature. 2012;488:106–10. [PubMed: 22820256]
10. Robinson G, Parker M, Kranenburg TA, Lu C, Chen X, Ding L, et al. Novel mutations target distinct subgroups of medulloblastoma. Nature. 2012;488:43–8. [PubMed: 22722829]
11. Kool M, Jones DT, Jager N, Northcott PA, Pugh TJ, Hovestadt V, et al. Genome sequencing of SHH medulloblastoma predicts genotype-related response to smoothened inhibition. Cancer Cell. 2014;25:393–405. [PubMed: 24651015]
12. Zhang L, He X, Liu X, Zhang F, Huang LF, Potter AS, et al. Single-Cell Transcriptomics in Medulloblastoma Reveals Tumor-Initiating Progenitors and Oncogenic Cascades during Tumorigenesis and Relapse. Cancer Cell. 2019;36:302–18 e7. [PubMed: 31474569]
13. Hovestadt V, Smith KS, Bihannic L, Filbin MG, Shaw ML, Baumgartner A, et al. Resolving medulloblastoma cellular architecture by single-cell genomics. Nature. 2019;572:74–9. [PubMed: 31341285]
14. Vladoiu MC, El-Hamamy I, Donovan LK, Farooq H, Holgado BL, Sundaravadanam Y, et al. Childhood cerebellar tumours mirror conserved fetal transcriptional programs. Nature. 2019;572:67–73. [PubMed: 31043743]
15. Yao M, Ventura PB, Jiang Y, Rodriguez FJ, Wang L, Perry JSA, et al. Astrocytic trans-Differentiation Completes a Multicellular Paracrine Feedback Loop Required for Medulloblastoma Tumor Growth. Cell. 2020;180:502–20 e19. [PubMed: 31983537]
16. Yi J, Shi X, Xuan Z, Wu J. Histone demethylase UTX/KDM6A enhances tumor immune cell recruitment, promotes differentiation and suppresses medulloblastoma. Cancer Letters. 2020.
17. Morrissy AS, Cavalli FMG, Remke M, Ramaswamy V, Shih DJH, Holgado BL, et al. Spatial heterogeneity in medulloblastoma. Nat Genet. 2017;49:780–8. [PubMed: 28394352]

18. Yi J, Wu J. Epigenetic regulation in medulloblastoma. Mol Cell Neurosci. 2018;87:65–76. [PubMed: 29269116]
19. Roussel MF, Stripay JL. Epigenetic Drivers in Pediatric Medulloblastoma. Cerebellum. 2018;17:28–36. [PubMed: 29178021]
20. Shi X, Wang Q, Gu J, Xuan Z, Wu JI. SMARCA4/Brg1 coordinates genetic and epigenetic networks underlying Shh-type medulloblastoma development. Oncogene. 2016;35:5746–58. [PubMed: 27065321]
21. Shi X, Zhang Z, Zhan X, Cao M, Satoh T, Akira S, et al. An epigenetic switch induced by Shh signalling regulates gene activation during development and medulloblastoma growth. Nat Commun. 2014;5:5425. [PubMed: 25370275]
22. Batora NV, Sturm D, Jones DT, Kool M, Pfister SM, Northcott PA. Transitioning from genotypes to epigenotypes: why the time has come for medulloblastoma epigenomics. Neuroscience. 2014;264:171–85. [PubMed: 23876321]
23. Dubuc AM, Remke M, Korshunov A, Northcott PA, Zhan SH, Mendez-Lago M, et al. Aberrant patterns of H3K4 and H3K27 histone lysine methylation occur across subgroups in medulloblastoma. Acta neuropathologica. 2013;125:373–84. [PubMed: 23184418]
24. Hock H A complex Polycomb issue: the two faces of EZH2 in cancer. Genes Dev. 2012;26:751–5. [PubMed: 22508723]
25. Martinez-Garcia E, Licht JD. Deregulation of H3K27 methylation in cancer. Nat Genet. 2010;42:100–1. [PubMed: 20104248]
26. Zhang H, Zhu D, Zhang Z, Kaluz S, Yu B, Devi NS, et al. EZH2 targeting reduces medulloblastoma growth through epigenetic reactivation of the BAI1/p53 tumor suppressor pathway. Oncogene. 2020;39:1041–8. [PubMed: 31582835]
27. Cheng Y, Liao S, Xu G, Hu J, Guo D, Du F, et al. NeuroD1 Dictates Tumor Cell Differentiation in Medulloblastoma. Cell reports. 2020;31:107782. [PubMed: 32579914]
28. Vo BT, Li C, Morgan MA, Theurillat I, Finkelstein D, Wright S, et al. Inactivation of Ezh2 Upregulates Gfi1 and Drives Aggressive Myc-Driven Group 3 Medulloblastoma. Cell reports. 2017;18:2907–17. [PubMed: 28329683]
29. Liu H, Sun Q, Sun Y, Zhang J, Yuan H, Pang S, et al. MELK and EZH2 Cooperate to Regulate Medulloblastoma Cancer Stem-like Cell Proliferation and Differentiation. Mol Cancer Res. 2017.
30. Yang H, Xie X, Deng M, Chen X, Gan L. Generation and characterization of Atoh1-Cre knock-in mouse line. Genesis. 2010;48:407–13. [PubMed: 20533400]
31. Ben-Arie N, Bellen HJ, Armstrong DL, McCall AE, Gordadze PR, Guo Q, et al. Math1 is essential for genesis of cerebellar granule neurons. Nature. 1997;390:169–72. [PubMed: 9367153]
32. Matei V, Pauley S, Kaing S, Rowitch D, Beisel KW, Morris K, et al. Smaller inner ear sensory epithelia in Neurog 1 null mice are related to earlier hair cell cycle exit. Developmental dynamics : an official publication of the American Association of Anatomists. 2005;234:633–50. [PubMed: 16145671]
33. Mao J, Ligon KL, Rakhlin EY, Thayer SP, Bronson RT, Rowitch D, et al. A novel somatic mouse model to survey tumorigenic potential applied to the Hedgehog pathway. Cancer Res. 2006;66:10171–8. [PubMed: 17047082]
34. Hayashi S, McMahon AP. Efficient recombination in diverse tissues by a tamoxifen-inducible form of Cre: a tool for temporally regulated gene activation/inactivation in the mouse. Dev Biol. 2002;244:305–18. [PubMed: 11944939]
35. Madisen L, Zwingman TA, Sunkin SM, Oh SW, Zariwala HA, Gu H, et al. A robust and high-throughput Cre reporting and characterization system for the whole mouse brain. Nat Neurosci. 2010;13:133–40. [PubMed: 20023653]
36. Xie H, Xu J, Hsu JH, Nguyen M, Fujiwara Y, Peng C, et al. Polycomb repressive complex 2 regulates normal hematopoietic stem cell function in a developmental-stage-specific manner. Cell Stem Cell. 2014;14:68–80. [PubMed: 24239285]
37. Zhan X, Shi X, Zhang Z, Chen Y, Wu JI. Dual role of Brg chromatin remodeling factor in Sonic hedgehog signaling during neural development. Proc Natl Acad Sci U S A. 2011;108:12758–63. [PubMed: 21768360]

38. Bray NL, Pimentel H, Melsted P, Pachter L. Near-optimal probabilistic RNA-seq quantification. Nat Biotechnol. 2016;34:525–7. [PubMed: 27043002]

39. McCarthy DJ, Chen Y, Smyth GK. Differential expression analysis of multifactor RNA-Seq experiments with respect to biological variation. Nucleic Acids Res. 2012;40:4288–97. [PubMed: 22287627]

40. Luo Z, Dong X, Yu J, Xia Y, Berry KP, Rao R, et al. Genomic and Transcriptomic Analyses Reveals ZNF124 as a Critical Regulator in Highly Aggressive Medulloblastomas. Front Cell Dev Biol. 2021;9:634056. [PubMed: 33681213]

41. Schuller U, Heine VM, Mao J, Kho AT, Dillon AK, Han YG, et al. Acquisition of granule neuron precursor identity is a critical determinant of progenitor cell competence to form Shh-induced medulloblastoma. Cancer Cell. 2008;14:123–34. [PubMed: 18691547]

42. Corcoran RB, Bachar Raveh T, Barakat MT, Lee EY, Scott MP. Insulin-like growth factor 2 is required for progression to advanced medulloblastoma in patched1 heterozygous mice. Cancer Res. 2008;68:8788–95. [PubMed: 18974121]

43. Rao G, Pedone CA, Del Valle L, Reiss K, Holland EC, Fults DW. Sonic hedgehog and insulin-like growth factor signaling synergize to induce medulloblastoma formation from nestin-expressing neural progenitors in mice. Oncogene. 2004;23:6156–62. [PubMed: 15195141]

44. Northcott PA, Buchhalter I, Morrissy AS, Hovestadt V, Weischenfeldt J, Ehrenberger T, et al. The whole-genome landscape of medulloblastoma subtypes. Nature. 2017;547:311–7. [PubMed: 28726821]

45. Ivanov DP, Coyle B, Walker DA, Grabowska AM. In vitro models of medulloblastoma: Choosing the right tool for the job. J Biotechnol. 2016;236:10–25. [PubMed: 27498314]

46. Lim JS, Ibaseta A, Fischer MM, Cancilla B, O'Young G, Cristea S, et al. Intratumoural heterogeneity generated by Notch signalling promotes small-cell lung cancer. Nature. 2017;545:360–4. [PubMed: 28489825]

47. McGranahan N, Swanton C. Clonal Heterogeneity and Tumor Evolution: Past, Present, and the Future. Cell. 2017;168:613–28. [PubMed: 28187284]

48. Natarajan S, Li Y, Miller EE, Shih DJ, Taylor MD, Stearns TM, et al. Notch1-induced brain tumor models the sonic hedgehog subgroup of human medulloblastoma. Cancer Res. 2013;73:5381–90. [PubMed: 23852537]

49. Polesskaya A, Cuvellier S, Naguibneva I, Duquet A, Moss EG, Harel-Bellan A. Lin-28 binds IGF-2 mRNA and participates in skeletal myogenesis by increasing translation efficiency. Genes Dev. 2007;21:1125–38. [PubMed: 17473174]

Significance:

The identification of an oncogenic function of PRC2 heterogeneity in medulloblastoma provides insights into subclone competition and cooperation during heterogeneous tumor evolution.

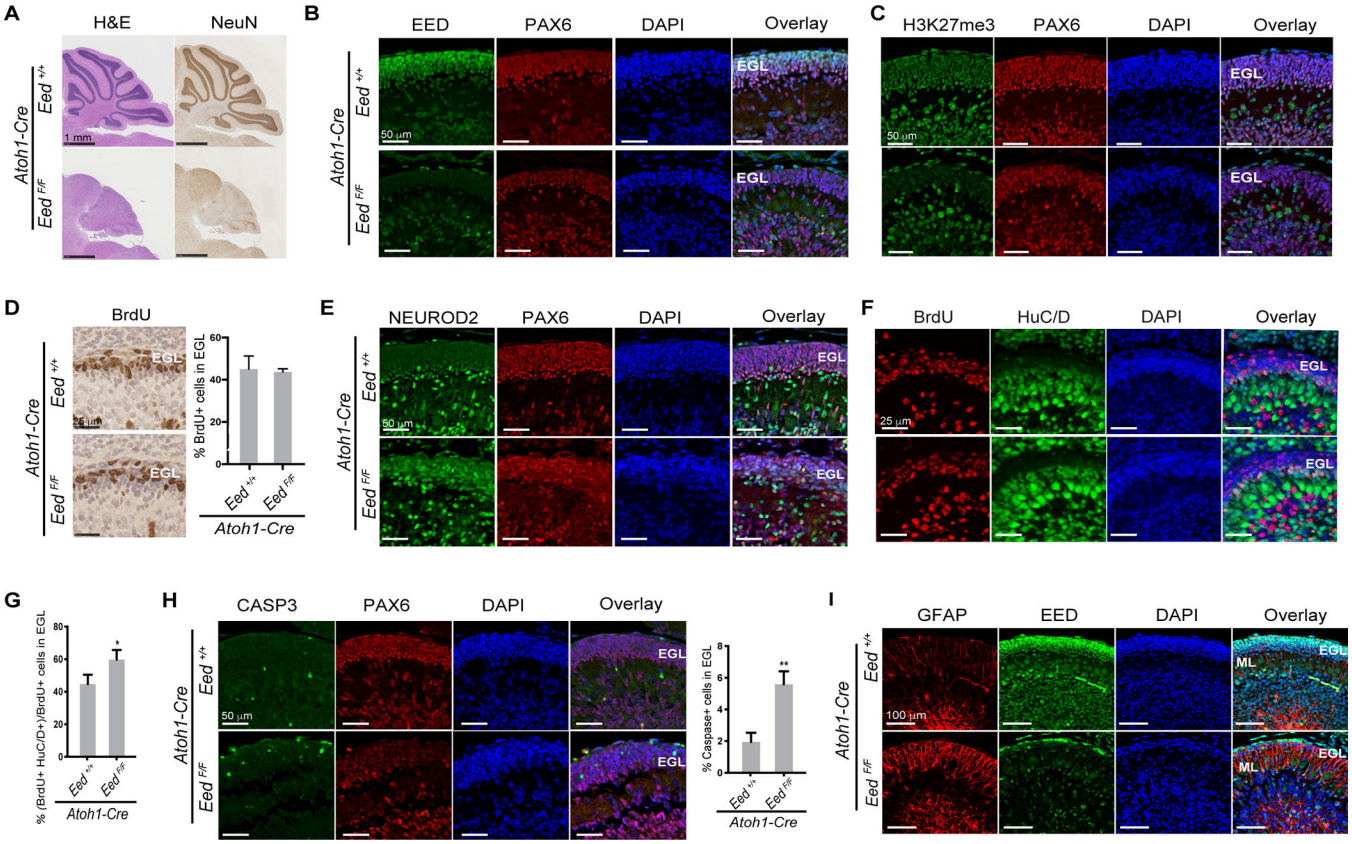

Figure 1. EED is required for cerebellar development.

A. H&E staining of sagittal sections of cerebella from *Atoh1-Cre Eed*$^{+/+}$ and *Atoh1-Cre Eed*$^{F/F}$ mice at P28. **B-I**. Representative pictures of immunostaining of sagittal sections of cerebella from *Atoh1-Cre Eed*$^{+/+}$ and *Atoh1-Cre Eed*$^{F/F}$ mice at P7 (**B, C, E, H, I**) and P2 (**D, F**). BrdU labeling was 30 min in **D** and 24 h in **F**. Quantifications are shown on the right except the quantification of F are shown in G (n=3). Student's t-test, *, $p<0.05$; **, $p<0.01$. EGL: external granule layer. ML: molecular layer. Please also see Figure S1.

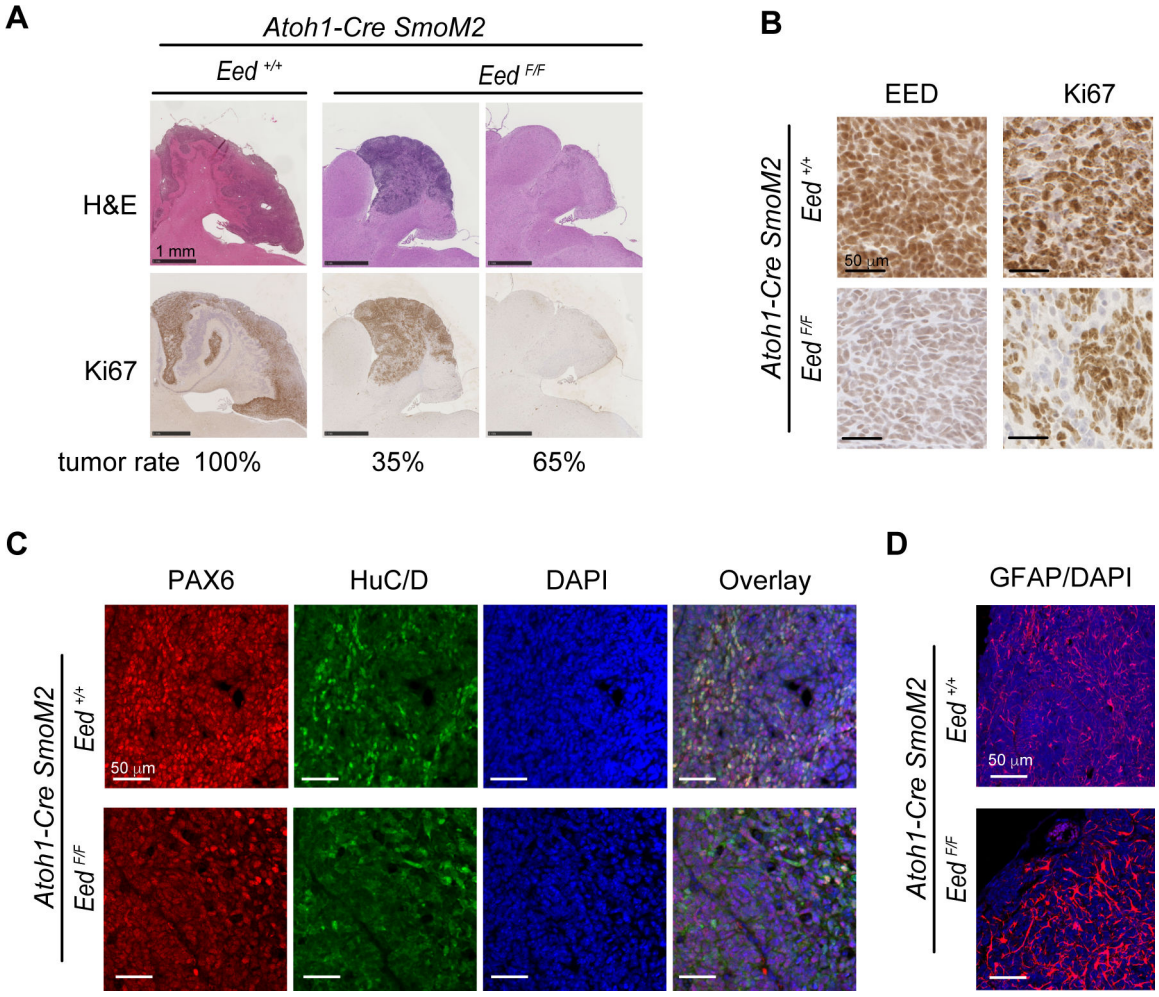

Figure 2. EED is required for medulloblastoma formation.

A. H&E and immunostaining of sagittal sections of cerebella from *Atoh1-Cre SmoM2 Eed*$^{+/+}$ mice and *Atoh1-Cre SmoM2 Eed*$^{F/F}$ mice at P60. Percentages under each genotype indicate their respective tumor occurrence rate (n=20 per group). **B-D**. Representative pictures of immunostaining of tumor sections of medulloblastomas from *Atoh1-Cre SmoM2 Eed*$^{+/+}$ and *Atoh1-Cre SmoM2 Eed*$^{F/F}$ mice.

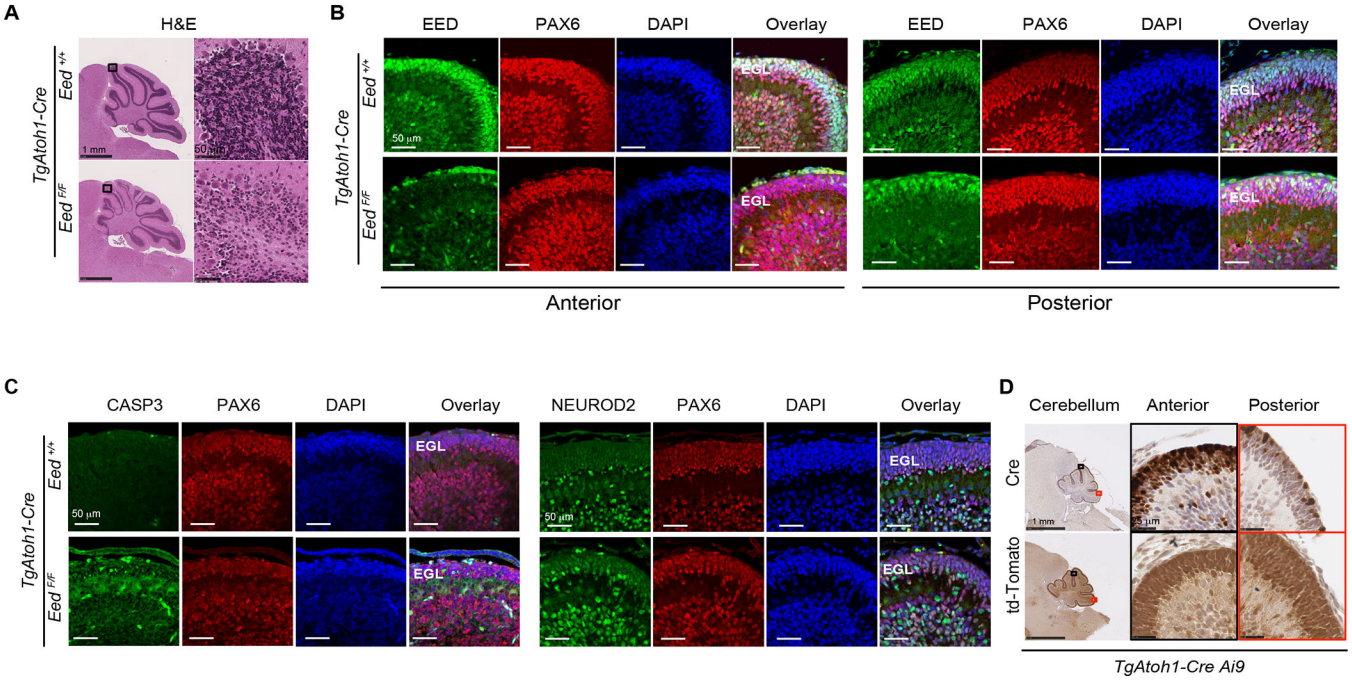

Figure 3. Heterogeneous TgAtoh1-Cre activities led to incomplete EED deletion and mild cerebellar defects.

A. H&E staining of sagittal sections of cerebella from P28 *TgAtoh1-Cre Eed*$^{+/+}$ and *TgAtoh1-Cre Eed*$^{F/F}$ mice. The boxed areas in the left pictures are shown on the right. **B-C**. Immunostaining of sagittal sections of cerebella from P7 *TgAtoh1-Cre Eed*$^{+/+}$ and *TgAtoh1-Cre Eed*$^{F/F}$ mice. Representative pictures show the staining of EED in the anterior and posterior regions (**B**), and cleaved Caspase 3 (CASP3) and NEUROD2 in the anterior region (**C**). **D.** Cre and td-Tomato staining of sagittal sections of cerebella from P2 *TgAtoh1-Cre Ai9* mice. Pictures on the right are boxed regions in the pictures on the left with corresponding outline colors. EGL: external granule layer. Please also see Figure S2.

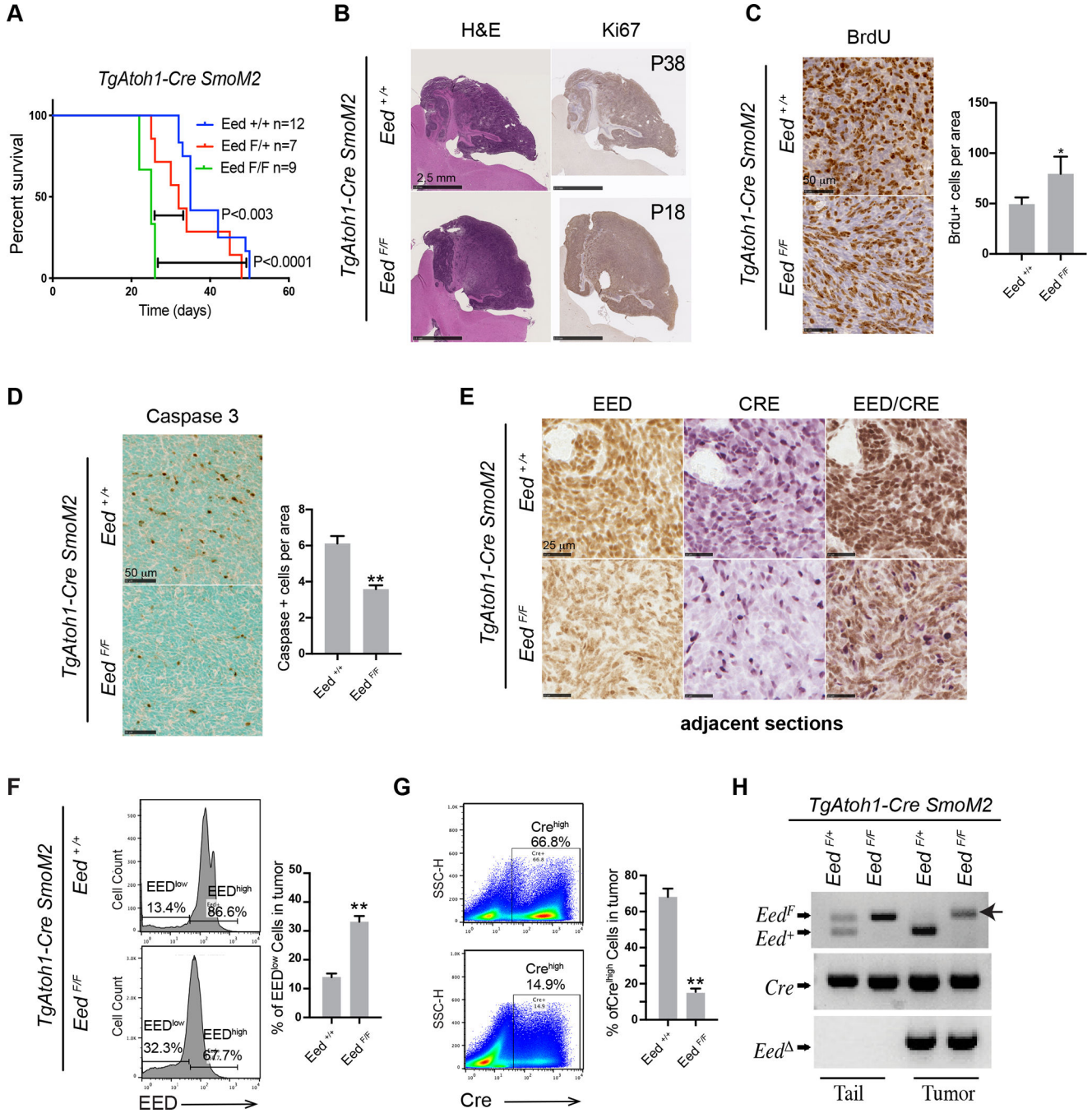

Figure 4. *TgAtoh1-Cre SmoM2 Eed*$^{F/F}$ mice showed enhanced tumor growth with mosaic EED deletion.

A. Survival curves of mice harboring *TgAtoh1-re SmoM2* medulloblastoma with indicated *Eed* genotypes. **B**. H&E and Ki67 staining of sagittal sections of tumor from *TgAtoh1-Cre SmoM2 Eed*$^{+/+}$ mice at P38 and *TgAtoh1-Cre SmoM2 Eed*$^{F/F}$ mice at P18. **C-E**. Immunostaining of sagittal sections of tumor from P18 *TgAtoh1-Cre SmoM2 Eed*$^{+/+}$ and *TgAtoh1-Cre SmoM2 Eed*$^{F/F}$ mice. Quantification is shown on the right (n=4). BrdU labeling time was 30 min in **C**. **F-G**. Flow cytometric analyses of EED (**F**, histograms,

n=3) and Cre (**G**, dot plots, n=3) distribution in tumors from P18 *TgAtoh1-Cre SmoM2 Eed*$^{+/+}$ and *TgAtoh1-Cre SmoM2 Eed*$^{F/F}$ mice. **H.** PCR genotyping of tail and tumor tissues from *TgAtoh1-Cre SmoM2 Eed*$^{F/+}$ and *TgAtoh1-Cre SmoM2 Eed*$^{F/F}$ mice. The arrow points to the unrecombined *Eed*^{F} allele in the *TgAtoh1-Cre SmoM2 Eed*$^{F/F}$ tumor. Student's t-test, *, $p<0.05$; **, $p<0.01$. Please also see Figure S2.

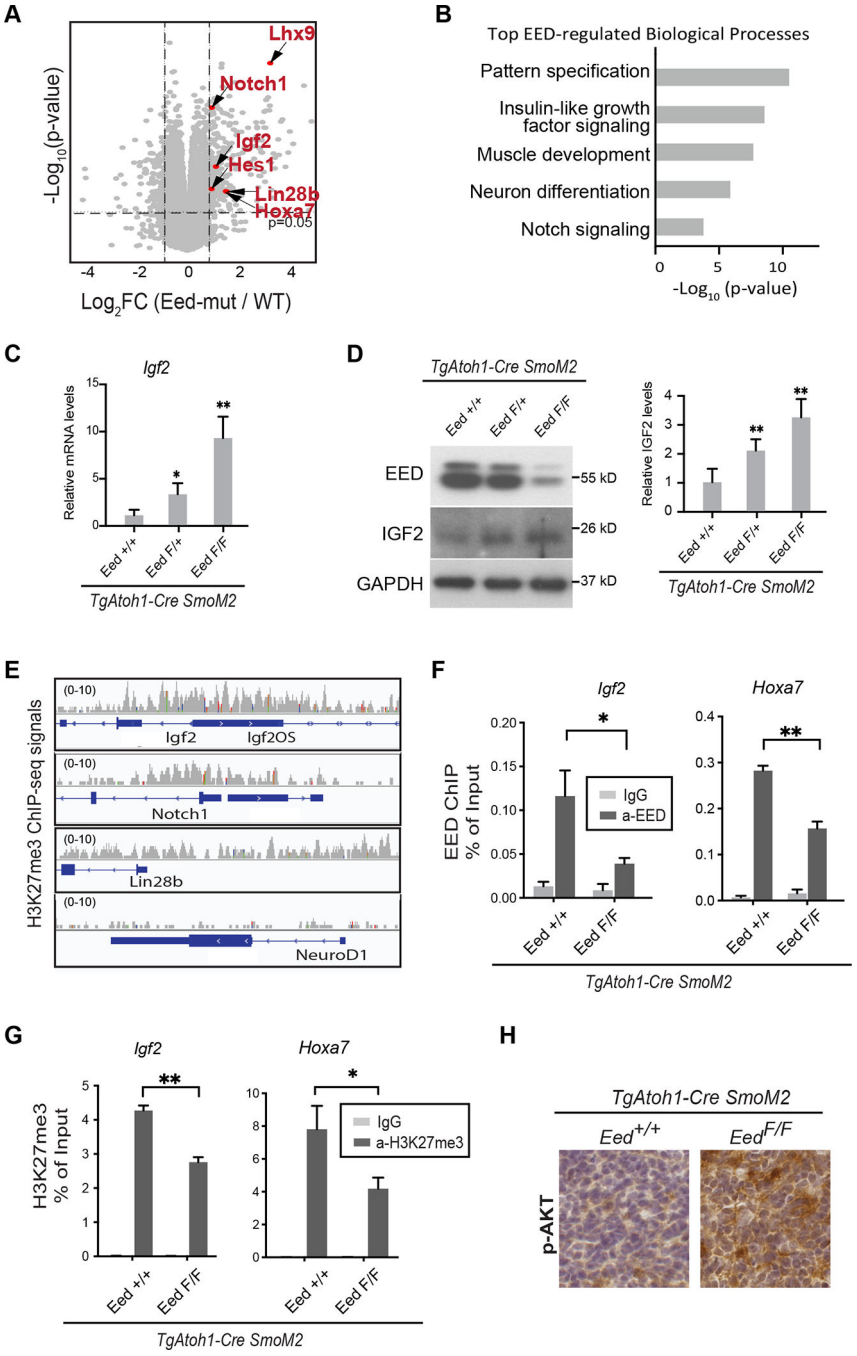

Figure 5. ***Igf2* is a PRC2 target that was derepressed in *TgAtoh1-Cre SmoM2 Eed$^{F/F}$* tumor.**

A. Volcano plot of RNA-seq data comparing *TgAtoh1-Cre SmoM2 Eed$^{+/+}$* (WT) and *TgAtoh1-Cre SmoM2 Eed$^{F/F}$* (*Eed-mut*) tumors. Red-labelled dots are known oncogenes increased in *Eed-mut* tumors. **B.** Gene ontology analysis of enriched pathways in up-regulated genes in *EED-mut* tumors. **C.** RT-qPCR of *Igf2* expression in *TgAtoh1-Cre SmoM2 Eed$^{+/+}$*, *Eed$^{F/+}$*, and *Eed$^{F/F}$* tumors (n=6). **D.** Western blot of IGF2 protein expression in *TgAtoh1-Cre SmoM2 Eed$^{+/+}$*, *Eed$^{F/+}$*, and *Eed$^{F/F}$* tumors. The quantification of IGF2 signals relative to GAPDH levels is shown on the right (n=3). **E.** H3K27me3 ChIP-

seq signals for *Igf2, Notch1,* and *Lin28b*. *NeuroD1* was used as an H3K27me3 negative control. **F-G.** ChIP-qPCR analysis of EED (**E**) and H3K27me3 (**F**) at the promoter regions of *Igf2* and *Hoxa7* (n=3) in *TgAtoh1-Cre SmoM2 Eed*$^{+/+}$ and *TgAtoh1-Cre SmoM2 Eed*$^{F/F}$ tumors. **H.** p-AKT staining of sections of tumors from *TgAtoh1-Cre SmoM2 Eed*$^{+/+}$ and *TgAtoh1-Cre SmoM2 Eed*$^{F/F}$ mice. Student's t-test, *, $p<0.05$; **, $p<0.01$. Please also see Figure S3.

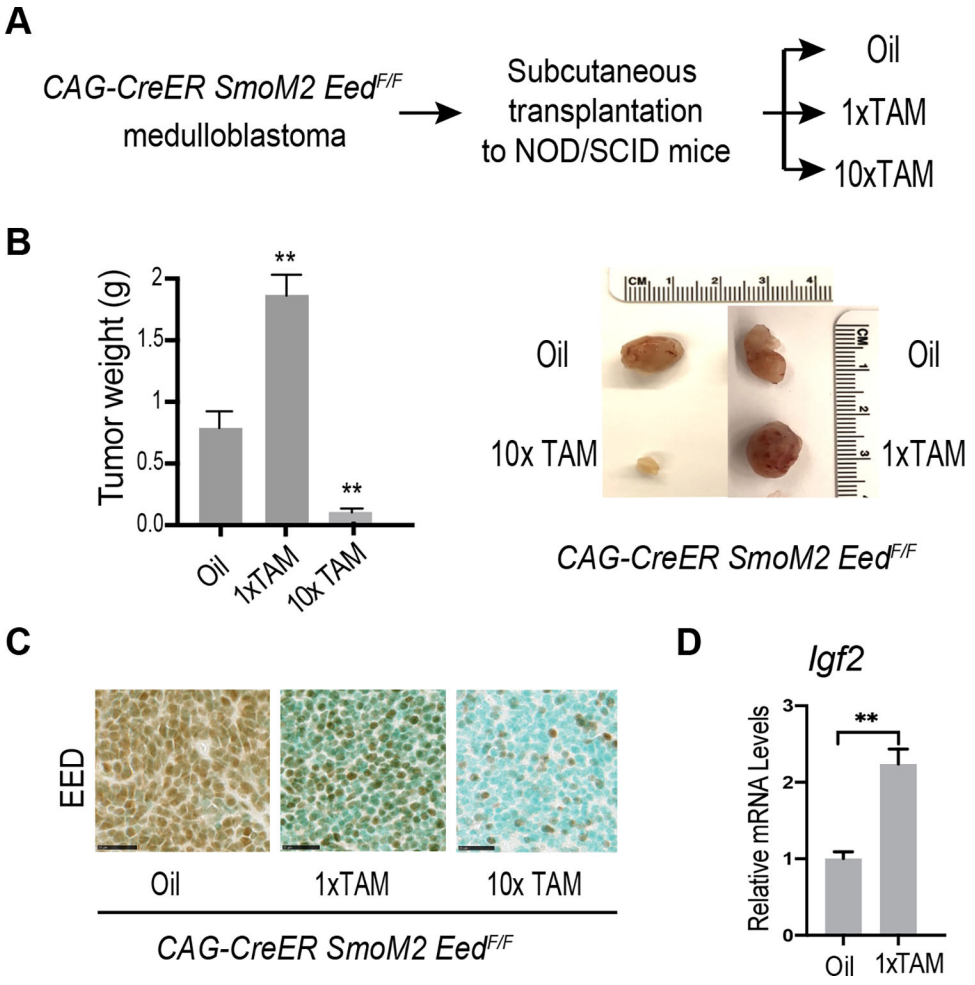

Figure 6. Second mouse model demonstrating the oncogenic function of PRC2 heterogeneity.

A. Experimental scheme of deleting EED completely or mosaically after SHH medulloblastoma tumor formation. **B.** Comparison of the growth of *CAG-CreER SmoM2 Eed*$^{F/F}$ medulloblastoma transplanted subcutaneously to NOD/ SCID mice treated with either oil, one or 10 doses of TAM (n=3). Representative images of transplanted tumors are shown on the right. **C.** EED staining of sections of transplanted tumors from NOD/ SCID mice treated with either oil, one or 10 doses of TAM. **D.** RT-qPCR of *Igf2* expression comparing tumors from NOD/ SCID mice treated with either oil or one dose of TAM (n=3).

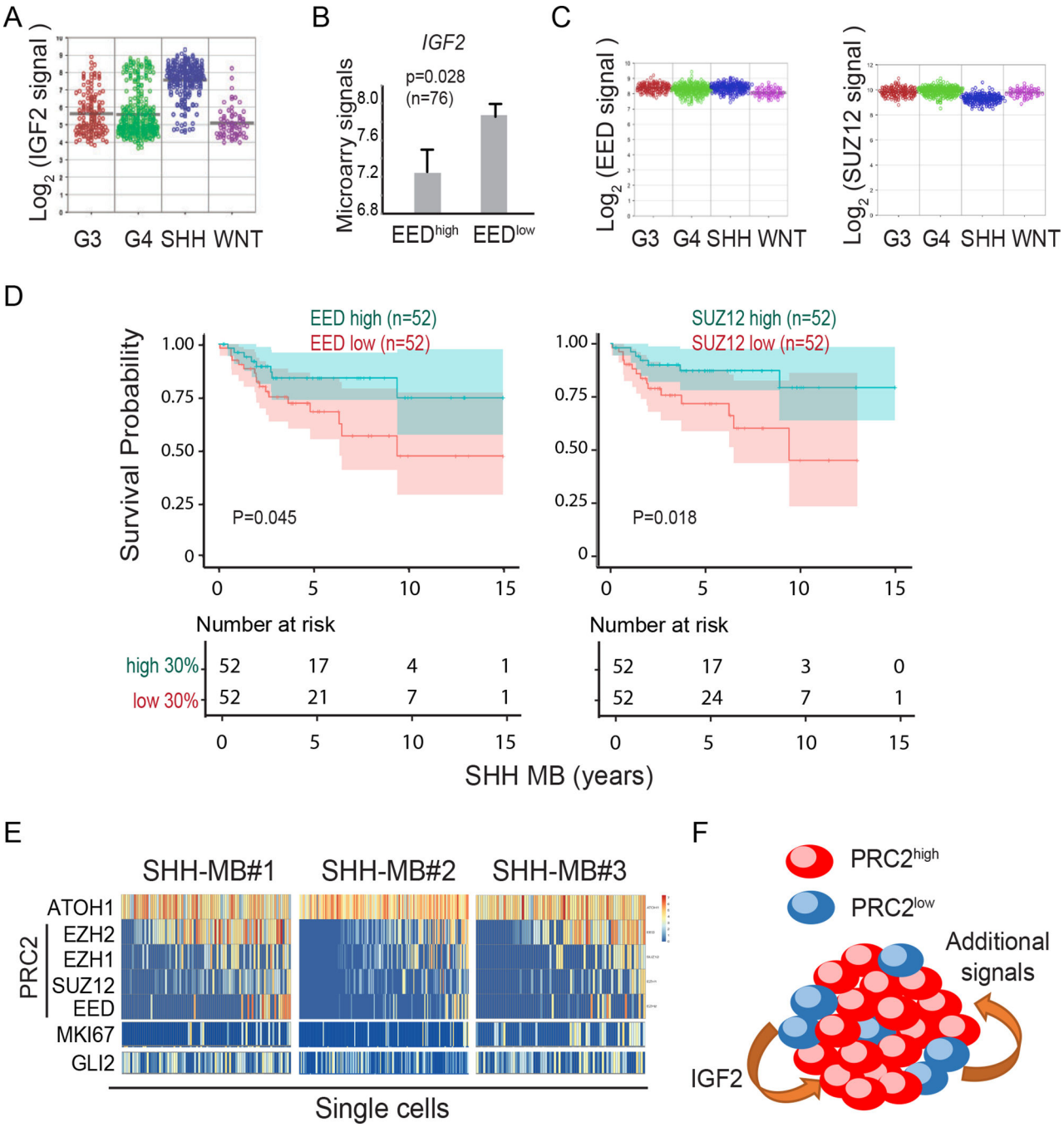

Figure 7. PRC2 heterogeneity and IGF2 expression in human medulloblastoma samples.

A. RNA-seq signals of *IGF2* among different subgroups of human medulloblastoma (n=172). **B.** *IGF2* levels are inversely related to *EED* in human SHH medulloblastoma. Shown are average microarray signals of *IGF2* in SHH medulloblastomas with high or low EED levels (n=76) (11). **C.** RNA-seq signals of *EED* and *SUZ12* among different subgroups of human medulloblastoma (n=172). **D.** Kaplan-Meier curves with 95% confidence interval of human SHH medulloblastoma with different levels of *EED* expression (left) and *SUZ12* (right) (n=172). Shown are the comparisons between the top 30% and bottom 30% of

patients ranked by *EED* or *SUZ12* tumor expression. **E.** Heatmap showing the expression of PRC2 subunits, *MKI67* and *GLI2* in all the *ATOH1*$^{+}$ cells in the Smart-seq of the 3 human SHH medulloblastoma samples (13). Each column represents a single cell and the columns are arranged according to the sum of PRC2 subunit levels. Blue indicates undetectable levels. **F.** The medulloblastoma subclone cooperation model. In a heterogeneous tumor that contains both PRC2^{high} and PRC2^{low} cells, the PRC2l^{ow} subclones, despite a lower growth competence, enhance PRC2^{high} subclone growth through derepressed secreted growth factors such as IGF2.

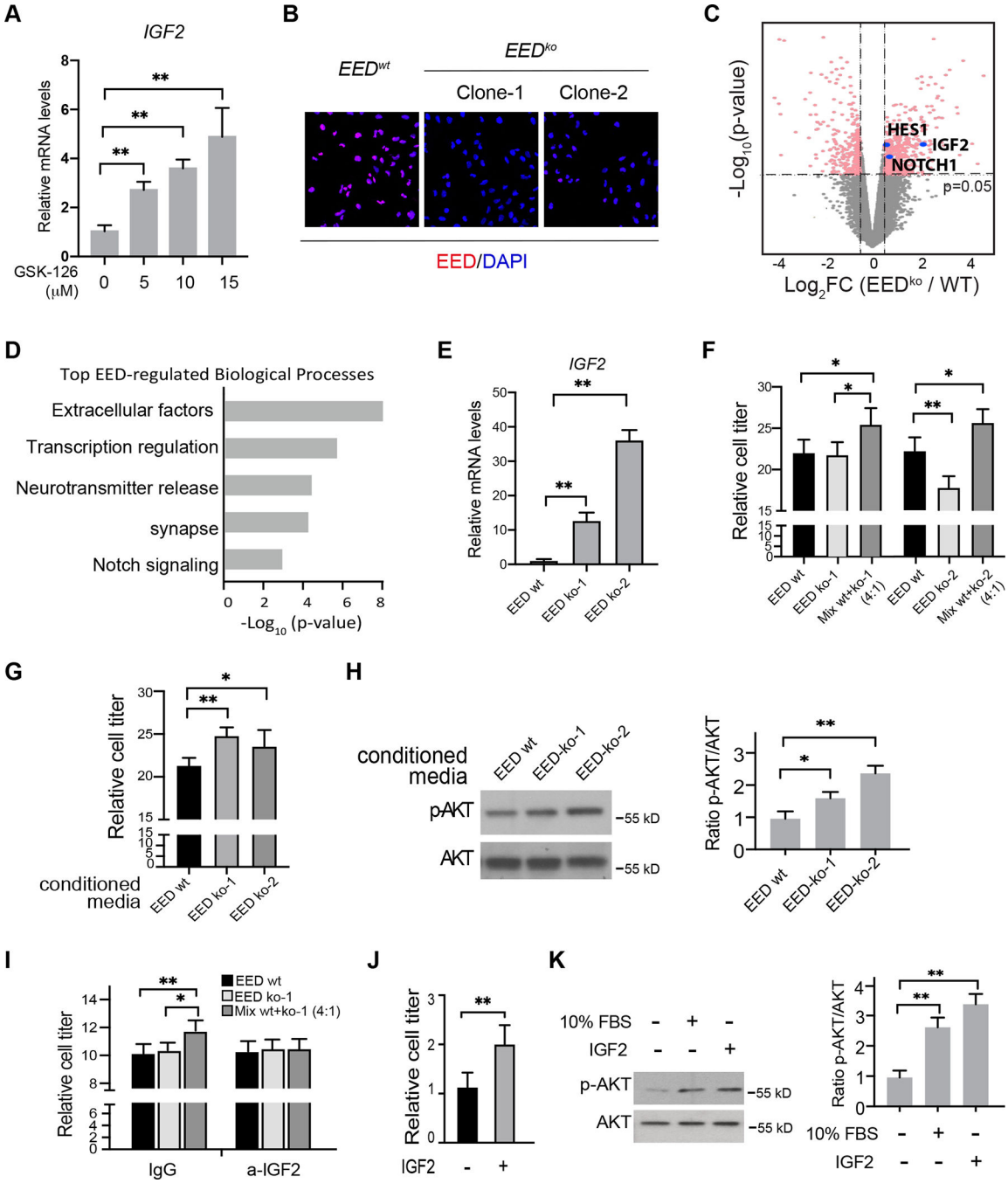

Figure 8. An IGF2/PI3K/AKT pathway mediated non-cell autonomous tumor suppressor function of EED in human medulloblastoma Daoy cells.

A. RT-qPCR of *IGF2* expression in Daoy cell treated with different doses of GSK-126 for 72 hours (n=6). **B.** EED staining of EED^{wt} and EED^{ko} Daoy cell clones generated by CRISPR-Cas9 system. **C.** Volcano plot of RNA-seq data comparing EED^{KO} with EED^{wt} (n=2). **D.** Gene ontology analysis of enriched pathways in up-regulated genes in EED^{KO} cells. **E.** RT-qPCR of *IGF2* expression in EED^{wt} and EED^{ko} Daoy cells (n=4). **F.** Cell viability assay of EED^{wt} and EED^{ko} Daoy cells culturing separately or in a 4:1 mixture

(n=5, 72 hours). **G.** Cell viability assay of Daoy cells cultured with conditioned media collected from EED^{wt} or EED^{ko} cultures (n=5). **H.** Western blot showed p-AKT and AKT levels in cells cultured with conditioned media collected from EED^{wt} or EED^{ko} cultures. The quantification is shown on the right (n=3). **I.** Cell viability assay of EED^{wt} or EED^{ko} or mixed cultures with an IGF2 neutralizing antibody or mouse IgG control (n=5). **J.** Cell viability assay of Daoy cells in the absent or present of 200 ng/ml recombinant IGF2 (n=5). **K.** Western blot showed p-AKT levels in Daoy cells in different culture conditions. The quantification is shown on the right (n=3). Student's t-test, *, $p<0.05$; **, $p<0.01$.